

Chapter 11

The Coupling of the Weather Research and Forecasting Model with the Urban Canopy Models for Climate Simulations



Zahra Jandaghian and Umberto Berardi

11.1 Introduction

The urbanization leads to alteration in the land surface characteristics and contributes to the alteration of climate (Akbari and Kolokotsa 2016). Built structures affect the transfer of momentum, turbulence, and thermal among the lower boundary layer (surfaces) and upper boundary layer (atmosphere) of a city (Huang et al. 2019; Li and Zhou 2019). The regional meteorological conditions are influenced by the interactions occurring among surface characteristics, planetary boundary layer (PBL), and physical processes in the atmosphere (Berardi 2016; Roberge and Sushama 2018), which is already showing to impact the energy demand, and will do so even more in the future (Berardi and Jafarpur 2020).

It is well known that the surface and ambient temperatures are higher in urban areas compared to their neighbors, while the UHI has been reported to be responsible for human thermal discomfort and increasing building energy demand (Vahmani and Ban-Weiss 2016; Kim et al. 2018; Berardi and Taleghami 2018). The UHI is calculated by land surface and air temperature differences between urban and rural areas.

Worldwide an increasing interest exists around the importance of predicting the UHI phenomenon to investigate UHI mitigation strategies (Jato-Espino 2019). Mesoscale models are applied to illustrate the impacts of physical parameterizations and urban characteristics on the meteorological processes (Jandaghian and Akbari

Z. Jandaghian

Department of Architectural Science, Ryerson University, Toronto, ON, Canada
e-mail: zjandaghian@ryerson.ca

U. Berardi (✉)

BeTOP Lab, Faculty of Engineering and Architecture, Ryerson University,
Toronto, ON, Canada
e-mail: uberardi@ryerson.ca

2018a; Doan et al. 2019; Jandaghian and Berardi 2020b). For this scope, the Weather Research and Forecasting (WRF) model is employed to predict the surface and atmospheric phenomenon on regional climate. However, to precisely estimate the UHI intensity, the differences among surface or near-surface ambient temperatures must be investigated in the urban region and its neighborhoods. Thus, it has been proposed to couple the WRF with the urban canopy models (UCMs) to evaluate the extent of spatial and temporal variations in atmospheric variables (WRF-UCMs).

The WRF incorporates three types of urban canopy models (UCMs) to estimate the heat emissions and moisture fluxes from the urban to the atmosphere: slab (SB-UCM), single layer (SL-UCM), and multilayer (ML-UCM) models. Previous research demonstrated the effects of urbanizations on regional climate using the WRF-UCMs (Lin et al. 2008; Flagg and Taylor 2011; Vahmani and Ban-Weiss 2016; Jandaghian and Akbari 2018b). Results illustrated the potential of the WRF-UCMs to simulate the exchanges among the urban surfaces and the meteorological conditions that affect the regional climate. The SB-UCM and ML-UCM indicated similar results for the air temperature and wind speed during summer in Houston (Salamanca et al. 2011). Kusaka et al. showed that the SL-UCM results are more reliable compared to the SB-UCM (2012). It is worth mentioning that the proper choice of the UCMs is conditioned to the compatibility of the models, computational performance, and data required for the regional climate analyses. Therefore, to assess the impacts of urbanizations, a proper urban canopy model needs to be selected.

This chapter aims to describe the WRF and the UCM simulation preparations and processes and to shed light on the capabilities of the WRF-UCMs to simulate the UHI intensity in the GTA during the 2011 and 2018 heat wave periods. This chapter intends to provide comprehensive knowledge regarding mesoscale simulation processes as well as the urban canopy modeling for future urban climate studies.

11.2 Preparations for Mesoscale Simulations

Meteorological models use surface characteristics and initial and boundary conditions to solve a set of conservation equations, simulate the advection and diffusion of pollutants, and predict meteorological conditions, such as the air temperature, moisture, or wind speed. The online Weather Research and Forecasting (WRF) model considers a variety of meteorological and physical characteristics (cloud convection, water cycle, planetary boundary layer, and atmospheric and surface radiation) to predict weather conditions. The WRF is a mesoscale numerical weather prediction (NWP) system which is fully compressible and non-hydrostatic. The WRF can be coupled with the urban canopy models (UCMs) to simulate the thermal and humidity cycles from canopies to the atmosphere. The UCMs represent urban areas to precisely predict ambient temperature, wind speed, relative humidity, precipitation, and short-wave and long-wave radiations.

Figure 11.1 shows the flowchart of WRF with the urban canopy model for urban climate simulations. The terrestrial data and weather-gridded data are obtained from North America Regional Reanalysis (NARR). The preprocessing of WRF (called WPS) is used to define the domain and period of simulation and interpolates the NARR data into the domain of interest.

Figure 11.2 shows the simulation approach to accomplish the goals of WRF simulations consisting of preparation and processes phases. The preparation includes compiling and coupling of models and simulation steps, such as defining domain and period of simulation and collecting input data and measurement data. The processes refer to WRF and UCM simulations. Besides, data analysis is the main part of the process, including comparing the simulation results with measurements.

11.2.1 Compiling and Coupling of the Models

WRF simulations require significant preparation and computer resources. At the onset, one should make sure that the computer has sufficient memory capacity and a fast processing system to compile, couple, and carry out various simulations promptly. The first step to start simulations is to collect and couple the preprocessing system (WPS), data assimilation (DA), and advanced research WRF solver (ARW-WRF).

- **WRF Preprocessing System (WPS)**—WPS is applied primarily to predict real data. In WPS, the domain is defined, the terrestrial data is mapped, and the meteorological parameters are interpolated to the domain.
- **WRF Data Assimilation (WRF-DA)**—WRF-DA is used to inject observed data into the domain produced by the WPS. It accounts to engross the initial condi-

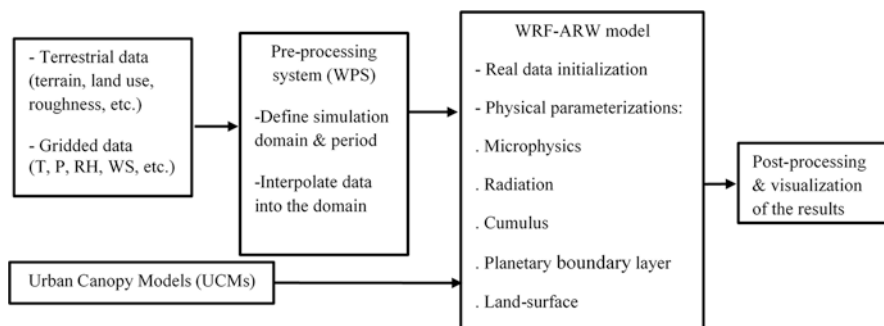


Fig. 11.1 Flowchart of WRF coupled with the urban canopy models (UCMs) (*T* temperature, *P* pressure, *RH* relative humidity, *WS* wind speed, *WPS* weather preprocessing system, *UCM* urban canopy model, *WRF* Weather Research and Forecasting model, *ARW* advanced research of the WRF)

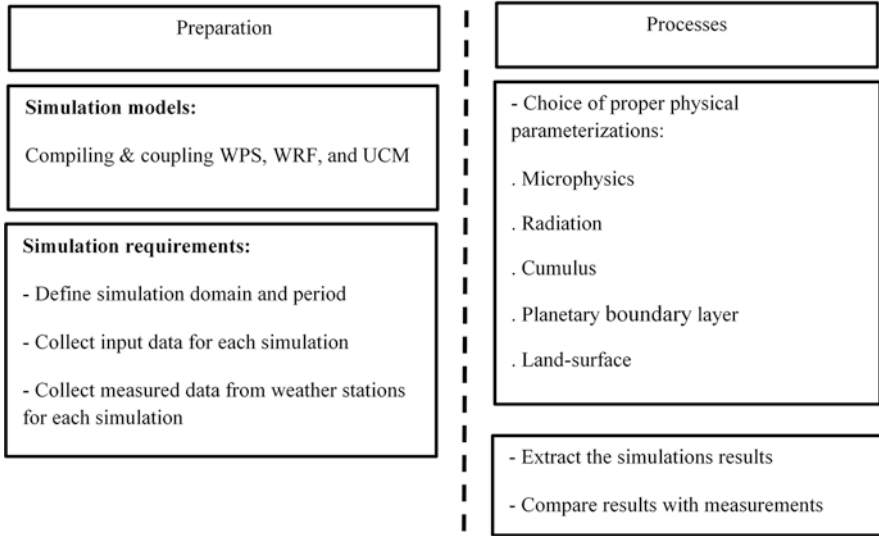


Fig. 11.2 Simulation preparation and processes (*WPS* weather preprocessing system, *WRF* Weather Research and Forecasting model, *UCM* urban canopy model)

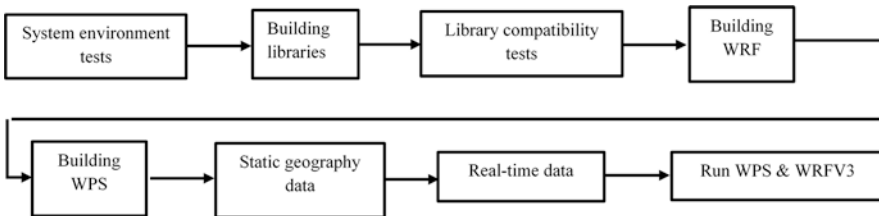


Fig. 11.3 Steps to compile and run the WPS and WRF models

tions into the WRF. The solver depends on data assimilation technique to simulate both 3D and 4D models.

- **Advanced Research WRF Solver (ARW-WRF)**—ARW-WRF is the main section of the modeling system and consists of several initialization programs. The key features consist of having the compressible, non-hydrostatic equations with hydrostatic choice. The solver can predict regional and global domains by using the mass-based terrain-following coordinates and vertical grid spacing.

Other features are the Runge-Kutta 2nd and 3rd order and 2nd to 6th order advection options, monotonic transport, and positive-definite advection option for moisture, scalar, tracer, and turbulent kinetic energy. Figure 11.3 shows the steps to

compile and run WPS and WRF. Table 11.1 summarizes the description of these steps.

- **Building WRFV4.** After ensuring that all libraries are compatible with the compilers, one can now prepare to build WRFV4. First, the tar file should be downloaded from a verified source (NCAR) and unpacked in the preferred directory. Then, a configuration file should be created to compile. The compiler is selected to be serial or in parallel. For parallel, which is for real case simulations, there are three options: “smpar,” “dmpar,” and “dm+sm.” The “dmpar” is the most proper

Table 11.1 Description of the steps to compile and run the WPS and WRF models

Steps to compile and run WPS and WRF models	Description
System environment tests	It is important to have the required compiler as gfortran. The WRF build system has scripts as the top level for the user interface as well
Building libraries	Various libraries should be installed, for example netcdf and Jasper. <i>These libraries must be installed with the same compilers as they will be used to install WRF and WPS</i>
Library compatibility tests	These tests are essential to verify that the libraries can work with the compilers that are to be used for the WPS and WRF builds
Building WRFV3	After ensuring that all libraries are compatible with the compilers, one can now prepare to build WRFV3. First, the tar file should be downloaded from a verified source and unpacked in the preferred directory. Then, a configuration file should be created to compile. The compiler is selected to be serial or in parallel
Building WPS	After building the WRF model, WPS program needs to be built. A tar file having the WPS source code is downloaded and unpacked. Then the WPS is compiled to be compatible with WRF. If the compilation is successful, there should be three executables in the WPS top-level directory that are linked to their corresponding directories
Static geography data	To initiate a real data case, the domain’s physical location on the globe and the static information for that location must be created. This requires a data set that includes such fields as topography and land use categories. These data need to be downloaded and uncompressed
Real-time data	For real data cases, the WRF model requires up-to-date meteorological information for both a first condition and lateral boundary conditions. This meteorological data is traditionally a file that is provided by a previously run external model or analysis. For a semi-operational setup, the meteorological data is usually sourced from a global model, which allows locating the WRF model’s domains anywhere on the globe
Run WPS and WRFV3	First, the WPS is executed by modifying its name list to reflect information that is required for the particular simulation. The geogrid will match the geographical data and define the simulation domain. The ungrid unpacks necessary data on the simulation period. The met grid interpolates the weather and terrestrial data on the domain of interest. To simulate the WRF, the name list needs to be changed. The data provided by WPS should be connected and linked to the run directory

possibility; it has fewer errors and is more compatible with other programming languages. To check whether it was successful, the executable files—namely “wrf.exe,” “real.exe,” “ndown.exe,” and “tc.exe”—need to be checked.

- **Building WPS.** After building the WRF model, WPS program needs to be built. A tar file containing the WPS source code is downloaded and unpacked. Then the WPS is compiled to be compatible with WRF. If the compilation is successful, there should be three executables in the WPS top-level directory, which are linked to their corresponding directories—namely “geogrid,” “ungrib,” and “metgrid.”
- **Static Geography Data.** To start a real data case, the domain physical location on the globe and the static information for that location must be created. This requires a data set that includes such fields as topography and land use categories. These data need to be downloaded and uncompressed.
- **Real-Time Data.** For real data cases, the WRF model requires up-to-date meteorological information for both an initial condition and lateral boundary conditions. This meteorological data is traditionally a Grib file that is provided by a previously run external model or analysis. For a semi-operational setup, the meteorological data is usually sourced from a global model, which permits locating the WRF model domains anywhere on the globe. The National Centers for Environmental Prediction (NCEP) run the Global Forecast System (GFS) model four times daily (initializations valid for 0000, 0600, 1200, and 1800 UTC). This is a global, isobaric, 0.5-degree latitude/longitude, forecast data set that is freely available and is usually accessible +4 h after the initialization time. A single data file needs to be acquired for each requested period.
- **Run WPS and WRFV3.** First, the WPS is executed by changing its “namelist.wps” to reflect the information that is needed for the simulation. The “geogrid.exe” will match the geographical data and define the simulation domain. The “ungird.exe” unpacks necessary data regarding the simulation period. The “metgird.exe” interpolates the weather and terrestrial data in the domain of interest. To simulate the WRF, the “namelist.input” needs to be modified. The data provided by WPS should be connected and linked to the run directory. First, the “real.exe” is executed and then the “WRF.exe.” The “error.rsl” file needs to be checked for any errors. If the execution was successful, then the required data should be extracted and analyzed. The physical parameterizations used in WRF include planetary boundary layer, short-wave and long-wave radiation, microphysics, cumulus, and land surface schemes.

11.2.2 Parametric Simulations of Physical Options

The physical parameterizations need to be carefully selected to predict weather conditions. A proper simulation platform provides a reliable opportunity to investigate the effects of UHI on meteorological parameters for environmental policymakers. A land surface model (LSM) predicts momentum and thermal and humidity cycles on

land points through atmospheric feedbacks of other schemes. LSM updates surface parameters in every time step.

- **Microphysics Scheme.** The microphysics scheme predicts the water cycle in the domain of interest. Water vapor initiates cloud water and cloud ice to produce snow, graupel, and rain. A set of conservation equations are applied to predict the water budget during the modeling period. Table 11.2 presents a brief description of the different schemes of microphysics in WRF.
- **Cumulus Scheme.** Cumulus scheme evaluates the impacts of convective air movement on up-drafting and down-drafting of clouds (Grell and Devenyi 2002). It influences the vertical thermal and humidity cycles in the simulation. The model identifies the convection, owes flux equations, and benefits from the closure assumptions. Table 11.3 presents a brief description of the different schemes of cumulus in WRF.

Table 11.2 Parameterization schemes of microphysics model in WRF

Scheme	Description
Lin	Applies the conservation equations and predicts source and sink of snow, hail, and rain
SBU-YLin	Predicts ice and snow
Eta	Considers six species of water
WRF Single-Moment 6-class	Has more accurate dependency of snow to temperature
WRF Double-Moment 6-class	Considers the mixing ratio and number concentration as independent variables
Thompson	Predicts the mixing ratios of five hydrometeors and the concentration of cloud ice
Morrison	Considers five species of water and predicts the mixing ratio
Severe Storms Laboratory	Considers lightning in microphysical models
Goddard	Calculates the condensation and deposition of cloud water and cloud ice
Milbrandt-Yau	Uses gamma size distribution

Table 11.3 Parameterization schemes of cumulus model in WRF

Scheme	Description
Simplified Arakawa-Schubert	Considers the mass and energy balance in clouds. Surface rainfall is parameterized in the moisture balance equation
Betts-Miller-Janjic	Considers convective mixing and predicts the shallow clouds
Grell 3D	Divides parameterizations into dynamic control and feedback
Grell-Freitas	Predicts the cloud convection in high-resolution grid size simulations
Kain-Fritsch	Simulates the water cycle instabilities
New Simplified Arakawa-Schubert	Considers the convection-induced pressure gradient forcing in the momentum equation
Tiedtke	Considers the eddy transport of energy in prognostic equations
Zhang-McFarlane	Considers the exchange of unstable air change with adjacent layers

Table 11.4 Parameterization schemes of planetary boundary layer models in WRF

Scheme	Description
Mellor-Yamada-Janjic (MYJ)	Considers the viscous sublayer above water bodies
Bougeault-Lacarrere (BouLac)	Calculates the TKE in a prognostic equation

- **Planetary Boundary Layer (PBL) Schemes.** PBL scheme accounts for vertical flux exchange in a grid cell. PBL predicts the impacts of momentum, heat, and moisture fluxes. PBL is divided into three sublayers: viscous layer, surface layer, and transition layer. Table 11.4 presents a brief description of the different schemes of PBL in WRF.
- **Radiation Scheme.** The radiation scheme calculates the energy balance. The short-wave radiation from the sun reaches the urban surfaces. The urban surface receives short-wave radiation as well as long-wave radiation from the sky and other structures. Urban absorbs a part of the radiation and reflects the remaining. The energy that reaches the surface is a function of sky condition and solar zenith angle. The long-wave radiation that is emitted from the urban surfaces goes through clouds and atmospheric gas or pollution.

11.3 Urban Canopy Models

The three urban canopy models can be coupled with the solver of the WRFV4.0: slab (SB-UCM), single-layer (SL-UCM), and multilayer (ML-UCM). The SL-UCM and ML-UCM consist of the three urban categories: low-intensity residential (with more than 20–70% vegetation cover), high-intensity residential (with less than 20% vegetation cover), and industrial/commercial areas.

11.3.1 Slab of the UCM

The SB-UCM applies roughness variables to simulate momentum and turbulence. The SB-UCM is a one-dimensional model assuming the buildings as bulk parameterizations and thus indicating the zero-order effects of urban surfaces (Liu et al. 2006). Here, the albedo is constant and the vegetation fraction is not accounted for. The PBL calculates the mixing length and vertical wind distribution (Chen and Dudhia 2001). The SB-UCM disregards the variability of urban structures.

The WRF includes the SB-UCM in NOAA parameterization. In the SL-UCM, the roughness length for momentum, over the building wall and over the ground, is assumed to be 0.0001 m and 0.01 m, respectively. Here, the albedo is 0.15, and the heat capacity for roof, wall, and road is $2.6 \text{ Jm}^{-3} \text{ K}^{-1}$. The thermal conductivity of urban surfaces is $3.14 \text{ Wm}^{-1} \text{ K}^{-1}$.

11.3.2 *Single Layer of the UCM*

The SL-UCM was developed to calculate the street canyons and building structure (Kusaka et al. 2001; Kanda et al. 2005). The SL-UCM accounts for a single orientation of the two-dimensional streets and estimates the three urban classes with various thermal characteristics. The SL-UCM estimates the sensible heat fluxes by assuming the wind distribution and evaluates the radiation processes in urban geometry. The SL-UCM accounts for the anthropogenic heat as a fixed temporal profile (Chen et al. 2011). In addition, the model considers the radiation behavior as shadowing, reflections, and trapping in the domain. The surface energy budget is applied to calculate the surface skin temperature. The thermal conduction equation estimates the temporal pattern. The Monin–Obukhov similarity theory calculates the surface-sensible heat fluxes. The sensible heat and momentum fluxes are conducted in the WRF-NOAH model. The canyon drag coefficient and friction velocity are analyzed. The anthropogenic heat and its diurnal variation are considered. The SL-UCM also accounts for the horizontal and vertical wind distribution in the canopy. The heat absorbed by urban surfaces and the sensible fluxes are defined as follows. The definition for each symbol is presented at the beginning of the chapter:

$$H_w = H_{w,s} + R_w \times H_{w,s} \times F_{w \rightarrow w} + R_G \times H_{G,s} \times F_{G \rightarrow w} \quad (11.1)$$

$$H_G = H_{G,s} + R_w \times H_{w,s} \times F_{G \rightarrow w} \quad (11.2)$$

$$\text{SHF}_a = \frac{2\tilde{h} \text{SHF}_w + \delta \text{SHF}_G}{\delta} \quad (11.3)$$

$$\text{SHF}_w = C_w (T_w - T_a) \quad (11.4)$$

$$\text{SHF}_G = C_G (T_G - T_a) \quad (11.5)$$

11.3.3 *Multilayer of the UCM*

The ML-UCM was developed to estimate the interaction of the buildings with the PBL (Martilli et al. 2002; Kondo et al. 2005) and thus named as the building effect parameterization (BEP). The ML-UCM simulates the three-dimensional canopy and calculates the vertical exchange of heat, moisture, and momentum (Salamanca et al. 2011). The model computes the TKE and energy and estimates heat emissions from the canopy by analyzing the drag force, diffusion factor, and radiations.

The ML-UCM accounts for the heterogeneous structure of the city and calculates the anthropogenic heat (AH) emissions that affect the UHI intensity estimation (Miao et al. 2009). The building energy model (BEM) is used to estimate the AH by

calculating the exchanges of energy between the interior of buildings and the outdoor atmosphere. The BEM accounts for the diffusion of heat from building surfaces, radiation exchanged through windows, long-wave radiation exchanged between indoor surfaces, and heat generations from occupants and equipment as well as air-conditioning, ventilation, and heating systems (Jandaghian and Berardi 2020a).

11.4 WRFV4.0 Configurations

The initial and boundary conditions were derived from the North American Regional Reanalysis (NARR) (Mesinger et al. 2006). The NOAA-LSM evaluates the boundary conditions for the meteorological model. The USGS 24-category is applied for the LULC data. The physical parameterization in the solver of the WRF is explained in the previous section. For these simulations, the Mellor-Yamada-Janjic scheme (Janjic 2002), the Goddard scheme, the rapid radiative transfer model—RRTMG (Iacono et al. 2008), and the Lin and Colle's (2011) and the Grell and Devenyi's (2002) schemes are, respectively, used to estimate the planetary boundary layer, short-wave and long-wave radiations, microphysics, and cumulus models. The moisture, scalars, and TKE are activated for model stability.

11.4.1 *Simulation Domain and Episode*

The Greater Toronto Area (GTA) is located at $\sim 43.7^\circ$ N and $\sim 79.3^\circ$ W and has more than six million inhabitants. The semi-continental climate of the GTA causes cold, long winters and hot, humid summers. High temperature and occurrences of heat waves in summer episode have negative influences on dwellers' health and comfort, especially on the vulnerable people as infants, elderly, and those with preexisting health conditions (Berardi 2016; Wang et al. 2016). Here, the simulations are composed of four two-way nested domains with the horizontal resolution of 9 km, 3 km, 1 km, and 0.333 km, respectively. The number of vertical layers is 51 eta level. Two heat wave periods are selected. The 2011 and 2018 heat wave periods started on the 17th and 1st of July, respectively, and lasted for 5 consecutive days. The 3 days of these periods are assessed as having the highest hourly maximum temperature (Jandaghian and Berardi 2020a).

11.4.2 *Model Performance Evaluation*

The WRF-UCM performance is evaluated by comparing the simulated results against measured data collected from urban and rural weather stations across the GTA in the heat wave period (21st–23rd of July) and 2018 heat wave period (3rd–5th

of July). Four weather stations are selected: Toronto City Centre, Pearson International Airport, Buttonville, and Oshawa. To practice model evaluation, mean bias error (MBE), mean absolute error (MAE), and root mean square error (RMSE) are calculated.

11.5 Results and Analyses

11.5.1 Ambient Temperature

The model evaluation of 2-m air temperature in four weather stations is presented in Table 11.5 showing the SB-UCM, SL-UCM, and ML-UCM. These comparisons show that the WRF-UCM predicts the temporal changes of 2-m air temperature precisely. The average MBE shows that the SB-UCM underestimated the ambient temperature during both heat wave events by $-1.4\text{ }^{\circ}\text{C}$ in 2011 and $-0.4\text{ }^{\circ}\text{C}$ in 2018. The SL-UCM underestimated the air temperature in 2011 ($\sim -1\text{ }^{\circ}\text{C}$), while slightly overestimated it in 2018 ($\sim 0.2\text{ }^{\circ}\text{C}$). The ML-UCM underestimated ambient temperature in 2011 ($\sim -1\text{ }^{\circ}\text{C}$) and overestimated it in 2018 ($\sim 1\text{ }^{\circ}\text{C}$) during the simulation period. However, the SL-UCM predicted the air temperature better in rural areas compared to urban region because it disregarded the anthropogenic heat emissions in its calculations.

Figure 11.4 presents the hourly comparisons of the air temperature with the measured data. The temporal variation of ambient temperature illustrates the same trend in both the SB-UCM and the SL-UCM simulations, but adding the heat emission

Table 11.5 The MBE, MAE, and RMSE of air temperature ($^{\circ}\text{C}$) in SB-UCM, SL-UCM, and ML-UCM at four weather stations over the GTA during the 2011 heat wave period (21st–23rd of July) and 2018 heat wave period (3rd–5th of July)

Station name	MBE ($^{\circ}\text{C}$)			MAE ($^{\circ}\text{C}$)			RMSE ($^{\circ}\text{C}$)		
	SB	SL	ML	SB	SL	ML	SB	SL	ML
<i>2011 Heat wave (21st–23rd of July)</i>									
Toronto City Center	-1.3	-1.1	-1.1	1.1	1.0	1.2	1.4	1.3	1.1
Pearson Int. Airport	-2.1	-1.2	-1.1	2.6	2.6	2.1	3.2	3.2	2.0
Buttonville	-0.7	0.5	-0.5	1.0	0.9	1.0	1.3	1.1	1.1
Oshawa	-1.4	-1.9	-1.5	1.5	1.2	1.1	1.7	1.6	1.7
Average	-1.4	-0.9	-1.0	1.6	1.4	1.1	1.9	1.8	1.4
<i>2018 Heat wave (3rd–5th of July)</i>									
Toronto City Center	-0.2	-0.1	1.0	0.7	1.2	1.4	0.8	1.4	1.7
Pearson Int. Airport	0.2	0.4	1.6	1.4	1.1	2.1	1.8	1.5	2.5
Buttonville	-1.1	-0.6	1.0	1.2	0.7	1.0	1.2	0.8	1.0
Oshawa	-0.4	1.2	1.3	1.1	1.2	1.3	1.3	1.5	1.6
Average	-0.4	0.2	1.2	1.1	1.1	1.5	1.3	1.3	1.7

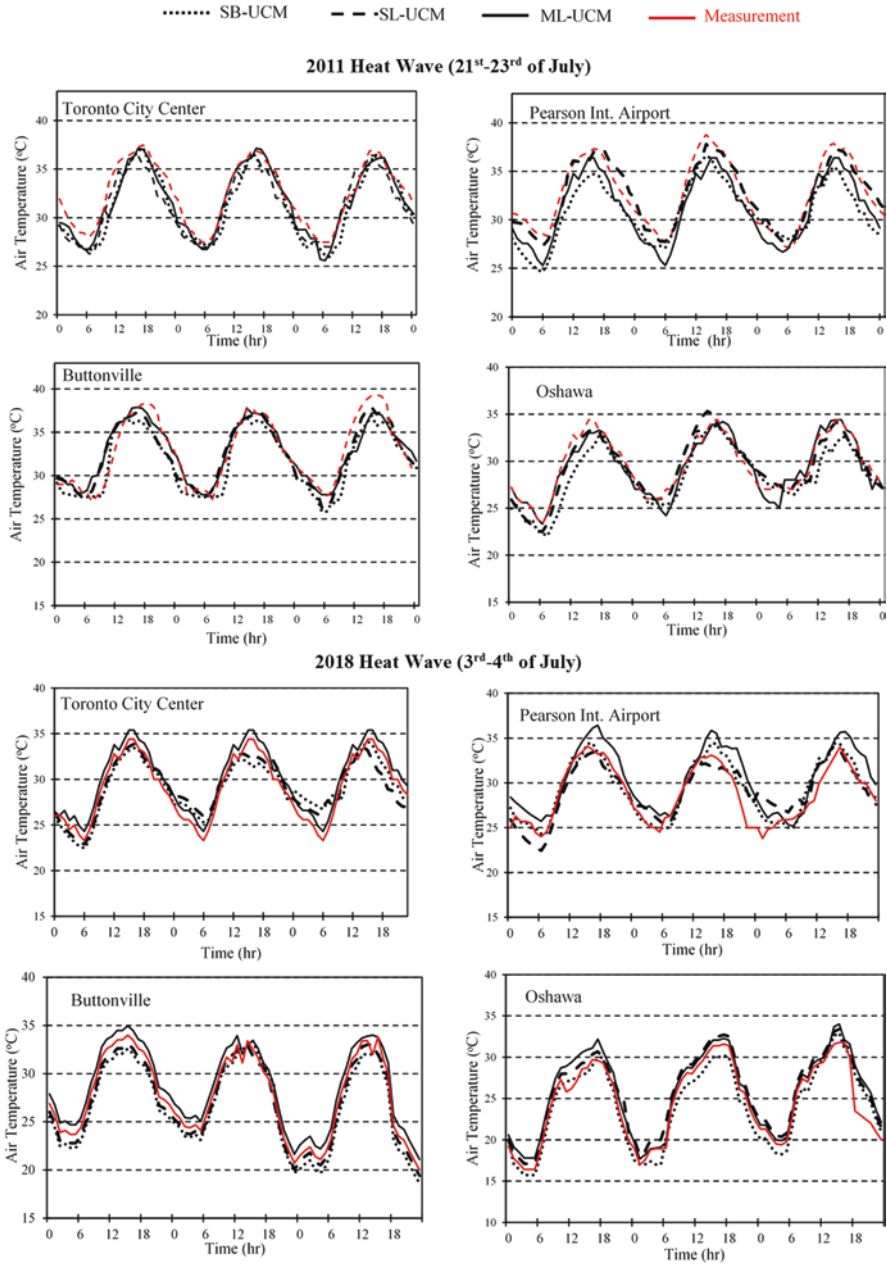


Fig. 11.4 Daily comparisons of 2-m air temperature (°C) in three UCMs vs. measured data from Toronto City Centre, Pearson Int. Airport, Buttonville, and Oshawa over the GTA during the 2011 heat wave period (21st–23rd of July) and 2018 heat wave period (3rd–5th of July)

from urban to the SL-UCM resulted in more accurate estimations. The correlation between the measurements and simulations is close to 0.9 and confirms the capability of the WRF-UCMs in forecasting air temperature efficiently. The results state that the SL-UCM and ML-UCM tend to slightly overpredict the temperature, but the hourly comparisons mark the more precise estimation of variables in the ML-UCM.

11.5.2 Wind Speed

Wind speed is underestimated in the SB-UCM (−2.4 m/s in 2011 vs. −0.4 m/s in 2018) and the SL-UCM (−1.6 m/s in 2011 vs. −0.8 m/s in 2018) simulations more compared to the ML-UCM (−1.5 m/s in 2011 vs. −0.1 m/s in 2018) (Table 11.6). The ML-UCM presents a better estimation of wind patterns. The reason is due to the capability of the ML-UCM to simulate the building height and street width. However, the daily comparisons of simulated results vs. measured data are not quite the same as the correlation close to 0.6. The reason is that the PBL cannot accurately predict the TKE and wind distribution for fine resolution grids. The largest underestimation of 10-m wind speed is seen in the SB-UCM because buildings and roughness impacts are dismissed. The average MAE of the UCMs in the domain is less or more the same for both heat wave events, but these criteria are slightly improved by applying the ML-UCM in urban canopy.

Table 11.6 The MBE, MAE, and RMSE of wind speed (m/s) in SB-UCM, SL-UCM, and ML-UCM at four weather stations over the GTA during the 2011 heat wave period (21st–23rd of July) and 2018 heat wave period (3rd–5th of July)

Station name	MBE (°C)			MAE (°C)			RMSE (°C)		
	SB	SL	ML	SB	SL	ML	SB	SL	ML
<i>2011 Heat wave (21st–23rd of July)</i>									
Toronto City Center	−1.5	−1.8	−2.2	2.4	3.8	4.6	3.4	4.3	5.1
Pearson Int. Airport	−4.5	−3.3	−3.6	5.9	5.2	5.2	6.8	6.0	6.0
Buttonville	−1.1	−0.7	−0.8	3.6	3.3	3.6	4.6	4.1	4.2
Oshawa	−2.6	−0.5	−0.5	4.1	2.8	2.9	4.8	3.3	3.0
Average	−2.4	−1.6	−1.5	4.0	3.8	4.1	4.9	4.4	4.2
<i>2018 Heat wave (3rd–5th of July)</i>									
Toronto City Center	0.4	−1.4	0.6	1.4	1.6	1.7	1.6	2.1	2.2
Pearson Int. Airport	−1.2	0.1	0.1	1.2	0.4	1.3	1.7	0.6	1.8
Buttonville	−1.3	−1.1	−0.6	1.3	1.1	1.1	1.8	1.7	1.7
Oshawa	0.7	−0.6	−0.4	1.0	0.8	0.6	1.6	1.3	0.9
Average	−0.4	−0.8	−0.1	1.2	1.0	1.2	1.7	1.4	1.7

11.5.3 Urban Heat Island Intensity

The urban heat island intensity (UHII) is considered as the difference in air temperature between urban and rural areas. In the mesoscale model, the ambient temperature depends on the surface temperature as urban fabric as well as sensible heat flux. The average daily, daytime, and nighttime urban-rural scale differences of ambient temperature are presented in Table 11.7. The results illustrate that the daily UHII is around 1.2–1.5 °C, while the daytime UHII is near 0.7–0.9 °C. The UHII is magnified during the night and reaches 2 °C and even 3 °C across the domain.

The averaged thermal pattern in the urban and rural areas of the GTA is presented in Fig. 11.5 during the simulations in 2011 and 2018 heat waves over the GTA. The daily pattern of air temperature illustrates that the nocturnal UHII is more evident, starting in the early evenings. The three UCMs simulate the changes in temperatures in urban and rural regions well. But the ML-UCM provides a more exact prediction of the UHII when compared against the measurements. It is worth mentioning that the location of the GTA close to the Lake Ontario has noticeable effects on regulating the air and skin temperatures even during the day and at around noon.

Table 11.7 The average daily, daytime, and nighttime urban heat island intensity of the SB-UCM, SL-UCM, ML-UCM, and measurement across the GTA during the 2011 heat wave period (21st–23rd of July) and 2018 heat wave period (3rd–5th of July)

Daily UHII				Daytime UHII				Nighttime UHII			
SB	SL	ML	Measured	SB	SL	ML	Measured	SB	SL	ML	Measured
<i>2011 Heat wave (21st–23rd of July)</i>											
1.35	1.35	1.46	1.34	0.85	0.82	0.91	0.89	3.11	3.16	2.94	2.11
<i>2018 Heat wave (3rd–5th of July)</i>											
1.47	1.35	1.39	1.26	0.77	0.73	0.71	0.58	2.28	1.92	2.09	1.88

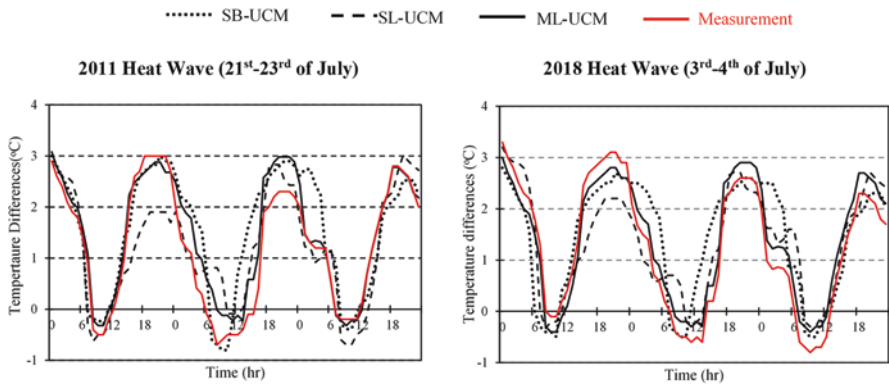


Fig. 11.5 Daily changes of 2-m air temperature (°C) in SB-UCM, SL-UCM, and ML-UCM results vs. measured data between urban and rural areas of the GTA during the 2011 heat wave period (21st–23rd of July) and 2018 heat wave period (3rd–5th of July)

11.6 Conclusions

To develop a platform to precisely analyze the urban climate and meteorological process in the GTA, a set of simulations are conducted. The WRF is coupled with the three urban canopy models separately. The simulations are run for two heat wave periods in 2011 and 2018. The results of these six base case simulations are compared with measured data from urban and rural weather stations. The aim to evaluate the integrated WRF-UCMs is to prepare the proper mesoscale model for urban climate simulations. The other goal is to accurately predict the impacts of urbanizations and climate change on urban structures, inhabitants, and environment. The growth of urbanization and climate change intensify the UHII impacts, increase the frequency and duration of the heat wave events, and deteriorate the regional air quality.

The WRF-UCMs forecast the temporal variation of air temperature reasonably well (the correlation between simulations and measurements is 0.9). In contrast, the prediction of wind speed requires more improvement in the mesoscale simulations (the correlation of the wind speed is 0.6). The SB-UCM underestimates the air temperature and wind speed because the model only estimates the zero-order impacts of structures and dismisses the vegetation cover.

The SL-UCM slightly overestimates air temperature and underestimates wind speed due to the miscalculations of the two-dimensional canopy, and estimation of fixed value for the anthropogenic heat emissions.

The ML-UCM overestimates air temperature and slightly underestimates wind speed. The ML-UCM simulation results are more reliable because it considers the three-dimensional urban surfaces and accounts for the vertical and horizontal exchange variables in urban canopy. The anthropogenic heat emissions are calculated and various building structures are considered in the urban canopy consisting of the influences of the radiation budget.

The UHI intensity is well characterized by the three UCMs. However, as it was expected, the ML-UCM simulates the diurnal variation of the ambient temperature more accurately. The analysis illustrated that the SL-UCM is reliable to simulate the urban climate, but for the precise evaluation of the UHII, the exact estimation in built-up structures is required that is satisfied via the ML-UCM model. It is worth mentioning that conducting the model with ML-UCM increases the computational time by 15%. These simulations illuminate the capability of the SL-UCM and ML-UCM in predicting the meteorological parameters and provide an urban climate platform to support assessing the impacts of UHI mitigation strategies in future studies.

Nomenclature

A	Area
C_p	Specific heat capacity
C_w	Convection heat transfer coefficient from walls to the canopy
E	Latent heat
$F_{w \rightarrow w}$	View factor from wall to wall
$F_{G \rightarrow w}$	View factors from ground to wall
g	Gravity
G	Convection heat transfer coefficient from the ground to the canopy
H_w	Total heat absorbed by walls
H_G	Total heat absorbed by ground
$H_{w,s}$	Heat absorbed by walls from sky
$H_{G,s}$	Heat absorbed by grounds from sky
\tilde{h}	Height of the wall
K	Von Karman constant
K_z	Turbulence coefficient
k	Unit vector in the z-direction
p	Pressure
q_i	Specific humidity
R_w	Reflectance of the wall
R_G	Reflectance of the ground
SHF_a	Sensible heat fluxes from the canopy to the atmosphere
SHF_w	Sensible heat fluxes from walls to the canopy
SHF_G	Sensible heat fluxes from the ground to the canopy
S_θ	Source/sink term for potential temperature
S_q	Source/sink term for specific humidity
T_w	Temperatures of wall
T_G	Temperatures of ground
T_a	Temperatures of atmosphere
u	Horizontal velocity
U	Advection
V	Wind speed
W	Vertical perturbation from turbulence
Z	Momentum roughness length
θ	Potential temperature
ρ	Density
δ	Width of the wall
Ω	Angular velocity of the earth

Acknowledgments Funding for this research was provided by the NSERC DG #2016-04904 and the Ontario Ministry of Research Innovation and Science (MRIS) through the ERA award.

References

- Akbari, H., & Kolokotsa, D. (2016). Three decades of urban heat islands and mitigation technologies research. *Energy and Buildings*, *133*, 834–842.
- Berardi, U. (2016). The outdoor microclimate benefits and energy saving resulting from green roofs retrofits. *Energy and Buildings*, *121*, 217–229.
- Berardi, U., & Jafarpur, P. (2020). Assessing the impact of climate change on building heating and cooling energy demand in Canada. *Renewable Energy and Sustainable Reviews*, *121*, 109681.
- Berardi, U., & Taleghami, M. (2018). The effect of pavement characteristics on pedestrians' thermal comfort in Toronto. *Urban Climate*, *24*, 449–459.
- Chen, F., & Dudhia, J. (2001). Coupling an advanced land surface–hydrology model with the Penn State–NCAR MM5 modeling system. Part I: Model implementation and sensitivity. *Monthly Weather Review*, *129*, 569–585.
- Chen, F., Kusaka, H., Bornstein, R., Ching, J., Grimmond, C., Grossman-Clarke, S., Loridan, T., Manning, K., Martilli, A., Miao, S., Sailor, D., Salamanca, F., Taha, H., Tewari, M., Wang, X., Wyszogrodzki, A., & Zhang, C. (2011). The integrated Wrf/urban modelling system: Development, evaluation, and applications to urban environmental problems. *International Journal of Climatology*, *31*, 273–288.
- Doan, V. Q., Kusaka, H., & Nguyen, T. M. (2019). Roles of past, present, and future land use and anthropogenic heat release changes on urban heat island effects in Hanoi, Vietnam: Numerical experiments with a regional climate model. *Sustainable Cities and Society*, *47*, 101479.
- Flagg, D. D., & Taylor, P. A. (2011). Sensitivity of mesoscale model urban boundary layer meteorology to the scale of urban representation. *Atmospheric Chemistry and Physics*, *11*, 2952–2972.
- Grell, G. A., & Devenyi, D. (2002). A generalized approach to parameterizing convection combining ensemble and data assimilation techniques. *Geophysical Research Letters*, *29*(14), 31–38.
- Huang, Q., Huang, J., Yang, X., Fang, C., & Liang, Y. (2019). Quantifying the seasonal contribution of coupling urban land use types on urban heat island using land contribution index: A case study in Wuhan, China. *Sustainable Cities and Society*, *44*, 666–675.
- Iacono, M. J., Delamere, J. S., Mlawer, E. J., Shephard, M. W., Clough, S. A., & Collins, W. D. (2008). Radiative forcing by long-lived greenhouse gases: Calculations with the AER radiative transfer models. *Journal of Geophysical Research*, *113*, 131–103.
- Jandaghian, Z., & Akbari, H. (2018a). The effects of increasing surface albedo on urban climate and air quality: A detailed study for Sacramento, Houston, and Chicago. *Climate*, *6*, 2–19.
- Jandaghian, Z., & Akbari, H. (2018b). The effects of increasing surface reflectivity on heat-related mortality in the Greater Montreal Area, Canada. *Urban Climate*, *25*, 135–151.
- Jandaghian, Z., & Berardi, U. (2020a). Analysis of the cooling effects of higher albedo surfaces during heat waves coupling the Weather Research and Forecasting model with building energy models. *Energy and Buildings*, *207*, 109–627.
- Jandaghian, Z., & Berardi, U. (2020b). Comparing urban canopy models for microclimate simulations in Weather Research and Forecasting Models. *Sustainable Cities and Society*, *55*, 102–025.
- Janjic, Z. (2002). *Nonsingular implementation of the Mellor-Yamada level 2.5 scheme in the NCEP meso model*. Camp Springs, MD: National Centers for Environmental Prediction.
- Jato-Espino, D. (2019). Spatiotemporal statistical analysis of the urban heat island effect in a Mediterranean region. *Sustainable Cities and Society*, *46*, 101427.
- Kanda, M., Kawai, T., Kanega, M., Moriwaki, R., Narita, K., & Hagishima, A. (2005). A simple energy balance model for regular building arrays. *Boundary-Layer Meteorology*, *116*, 423–443.
- Kim, H., Gu, D., & Kim, H. Y. (2018). Effect of urban heat island mitigation in various climate zones in the United States. *Sustainable Cities and Society*, *41*, 841–852.
- Kondo, H., Genchi, Y., Kikegawa, Y., Ohashi, Y., Yoshikado, H., & Komiyama, H. (2005). Development of a multilayer urban canopy model for the analysis of energy consumption in

- a big city: Structure of the urban canopy model and its basic performance. *Boundary-Layer Meteorology*, 116, 395–421.
- Kusaka, H., Kondo, H., Kikegawa, Y., & Kimura, F. (2001). A simple single-layer urban canopy model for atmospheric models: Comparison with multi-layer and slab models. *Boundary-Layer Meteorology*, 101, 329–358.
- Kusaka, H., Fei, C., Tewari, M., Dudhia, J., Gill, D. O., & Duda, M. G. (2012). Numerical simulation of urban heat island effect by the WRF model with 4-km grid increment: An inter-comparison study between the urban canopy model and the slab model. *Journal of the Meteorological Society of Japan*, 90, 33–45.
- Li, X., & Zhou, W. (2019). Spatial patterns and driving factors of surface urban heat island intensity: A comparative study for two agriculture-dominated regions in China and the USA. *Sustainable Cities and Society*, 48, 101518.
- Lin, Y., & Colle, B. A. (2011). A new bulk microphysical scheme that includes riming intensity and temperature-dependent ice characteristics. *Monthly Weather Review*, 139, 1013–1035.
- Lin, C., Chen, W., Liu, S. C., Liou, Y., Liu, G. R., & Lin, T. H. (2008). Numerical study of the impact of urbanization on precipitation over Taiwan. *Atmospheric Environment*, 42, 2934–2947.
- Liu, Y., Chen, F., Warner, T., & Basara, J. (2006). Verification of a mesoscale data-assimilation and forecasting system for the Oklahoma City area during the joint urban 2003 field project. *Journal of Applied Meteorology and Climatology*, 45, 912–929.
- Martilli, A., Clappier, A., & Rotach, M. (2002). An urban surface exchange parameterisation for mesoscale models. *Boundary-Layer Meteorology*, 104, 261–304.
- Mesinger, F., Dimego, G., Kalnay, E., Mitchell, K., Shafran, P. C., Ebisuzaki, W., Jovic, D., Woollen, J., Rogers, E., Berbery, E. H., Ek, M. B., Fan, Y., Grumbine, R., Higgins, W., Li, H., Lin, Y., Manikin, G., Parrish, D., & Shi, W. (2006). North American regional reanalysis. *Bulletin of the American Meteorological Society*, 87(3), 343–360.
- Miao, S., Chen, F., LeMone, M., Tewari, M., Li, Q., & Wang, Y. (2009). An observational and modeling study of characteristics of urban heat island and boundary layer structures in Beijing. *Journal of Applied Meteorology and Climatology*, 48(3), 484–501.
- Roberge, F., & Sushama, L. (2018). Urban heat island in current and future climates for the island of Montreal. *Sustainable Cities and Society*, 40, 501–512.
- Salamanca, F., Martilli, A., Tewari, M., & Chen, F. (2011). A study of the urban boundary layer using different urban parameterizations and high-resolution urban canopy parameters with WRF. *Journal of Applied Meteorology and Climatology*, 50, 1107–1128.
- Vahmani, P., & Ban-Weiss, G. A. (2016). Impact of remotely sensed albedo and vegetation fraction on simulation of urban climate in WRF-urban canopy model: A case study of the urban heat island in Los Angeles. *Journal of Geophysical Research—Atmospheres*, 121, 1511–1531.
- Wang, Y., Berardi, U., & Akbari, H. (2016). Comparing the effects of urban heat island effect mitigation strategies in the city of Toronto. *Energy and Buildings*, 114, 2–19.